18. L. Dou et al., in Proc. ECOC2012, paper Th.1.D.3 (2012).
19. N. K. Fontaine et al., in Proc. ECOC2013, paper Mo.3.D.5 (2013).
20. K. Solis-Trapala, T. Inoue, S. Namiki, in Proc. OFC2014, paper W3F.8 (2014).
21. X. Liu, A. R. Chraplyvy, P. J. Winzer, R. W. Tkach, S. Chandrasekhar, Nat. Photonics 7, 560–568 (2013).
22. T. Yoshida, T. Sugihara, K. Ishida, T. Mizuochi, in Proc. OFC2014, paper M3C.6 (2014).
23. N. Alic, E. Myslivets, E. Temprana, B. P. P. Kuo, S. Radic, J. Lightwave Technol. 32, 2690–2698 (2014).
24. E. Myslivets, B. P. P. Kuo, N. Alic, S. Radic, Opt. Express 20, 3331–3344 (2012).
25. See supplementary materials on Science Online.
26. N. S. Bergano, C. R. Davidson, J. Lightwave Technol. 13, 879–888 (1995).
27. J. G. Proakis, M. Salehi, Digital Communications (McGraw-Hill, New York, ed. 5, 2007).
28. S. M. Berber, IEEE Trans. Instrum. Meas. 53, 575–580 (2004).
29. N. S. Bergano, in Fiber Optic Telecommunications IV (Academic Press, San Diego, CA, 2002), pp. 154–197.
30. K. S. Turitsyn, S. A. Derevyanko, I. V. Yurkevich, S. K. Turitsyn, Phys. Rev. Lett. 91, 203901 (2003).
31. E. Agrell, A. Alvarado, G. Durisi, M. Karlsson, J. Lightwave Technol. 32, 2862–2876 (2014).
32. J. P. Gordon, L. F. Mollenauer, Opt. Lett. 15, 1351–1353 (1990).
33. J. P. Gordon, H. A. Haus, Opt. Lett. 11, 665–667 (1986).
34. www.fujitsu.com/downloads/MICRO/fme/documentation/c60.pdf
35. M. H. Taghavi, G. C. Papen, P. H. Siegel, IEEE Trans. Inf. Theory 52, 5008–5022 (2006).

OPTICS

Quantum spin Hall effect of light

Konstantin Y. Bliokh,[1,2]* Daria Smirnova,[2] Franco Nori[1,3]*

Maxwell's equations, formulated 150 years ago, ultimately describe properties of light, from classical electromagnetism to quantum and relativistic aspects. The latter ones result in remarkable geometric and topological phenomena related to the spin-1 massless nature of photons. By analyzing fundamental spin properties of Maxwell waves, we show that free-space light exhibits an intrinsic quantum spin Hall effect—surface modes with strong spin-momentum locking. These modes are evanescent waves that form, for example, surface plasmon-polaritons at vacuum-metal interfaces. Our findings illuminate the unusual transverse spin in evanescent waves and explain recent experiments that have demonstrated the transverse spin-direction locking in the excitation of surface optical modes. This deepens our understanding of Maxwell's theory, reveals analogies with topological insulators for electrons, and offers applications for robust spin-directional optical interfaces.

Solid-state physics exhibits a family of Hall effects with remarkable physical properties. The usual Hall effect (HE) and quantum Hall effect (QHE) appear in the presence of an external magnetic field, which breaks the time-reversal ($\mathcal{T}$) symmetry of the system. The HE induces charge current orthogonal to both the magnetic field and an applied electric field, whereas the QHE (1) involves distinct topological electron states, with unidirectional edge modes (charge-momentum locking), characterized by the topological Chern number (2).

The intrinsic spin Hall effect (SHE) can occur in $\mathcal{T}$-symmetric electron systems with spin-orbit interactions. It produces a spin-dependent transport of electrons orthogonal to the external driving force (3, 4). There is also the quantum spin Hall effect (QSHE) (5, 6), which is characterized by unidirectional edge spin transport—edge states with opposite spins propagating in opposite directions. Such topological states with spin-momentum locking gave rise to a new class of materials: topological insulators (7, 8).

Alongside the extensive condensed-matter studies of electron Hall effects, their photonic counterparts have been found in various optical systems. In particular, both the HE (9) and the QHE with unidirectional edge propagation (10, 11) have been reported in magneto-optical systems with broken $\mathcal{T}$-symmetry. Furthermore, because photons are relativistic spin-1 particles, they naturally exhibit intrinsic spin-orbit interaction effects, including Berry phase (12) and the SHE (13–15) stemming from fundamental spin properties of Maxwell equations (16).

The only missing part in the above optical Hall effects is the QSHE for photons. Recently, it was suggested that photonic topological insulators can be created in complex metamaterials structures (17–19). Here, we show that pure free-space light already possesses intrinsic QSHE, and simple natural materials (such as metals supporting surface plasmon-polariton modes) exhibit some features that resemble topological insulators. We show that the recently discovered transverse spin in evanescent waves (20, 21) and spin-controlled unidirectional excitation of surface or waveguide modes (22–27) can be interpreted as manifestations of the QSHE of light.

Propagating (bulk) free-space modes of Maxwell equations are polarized plane waves. Introduc-ing the complex amplitude $\mathbf{E}(\mathbf{r})$ of the harmonic electric field $\mathbf{E}(\mathbf{r},t) = \text{Re}[\mathbf{E}(\mathbf{r})e^{-i\omega t}]$, the plane-wave solution with wave vector $\mathbf{k} = k\bar{\mathbf{z}}$ is

$$\mathbf{E} \propto \mathbf{e}\,\exp(ikz), \quad \mathbf{e} = \alpha\bar{\mathbf{x}} + \beta\bar{\mathbf{y}} \qquad (1)$$

Here, $k = \omega/c$, $\mathbf{e}$ is the complex unit polarization vector ($|\alpha|^2 + |\beta|^2 = 1$), whereas $\bar{\mathbf{x}}$, $\bar{\mathbf{y}}$, and $\bar{\mathbf{z}}$ denote the unit vectors of the corresponding axes. The Jones vector $\xi = (\alpha,\beta)^T$ is a three-dimensional (3D) spinor, which describes the SU(2) polarization state of light. The spin states of propagating light are circular polarizations $\xi = (1,\pm i)^T/\sqrt{2}$, with helicities $\sigma \equiv 2\text{Im}(\alpha^*\beta) = \pm 1$. According to the massless nature of photons, the plane-wave spin is directed along the wave vector: $\mathbf{S} = \sigma\mathbf{k}/k$ [we consider the spin density per photon in $\hbar = 1$ units (supplementary text)].

Generalizing Eq. 1 to an arbitrary direction of propagation, the polarization vector becomes momentum-dependent: $\mathbf{e}(\mathbf{k})$. Namely, it is tangent to the $\mathbf{k}$-space sphere because of the transversality condition $\mathbf{E} \cdot \mathbf{k} = 0$. This spherical $\mathbf{k}$-space geometry underlies the spin-orbit interaction of light (12–16). In particular, introducing the helicity basis of circular polarizations $\mathbf{e}^\sigma(\mathbf{k})$ (16), one can calculate the Berry connection $\mathbf{A}^{\sigma\sigma'} = -i\mathbf{e}^\sigma \cdot (\nabla_{\mathbf{k}})\mathbf{e}^{\sigma'}$ and curvature $\mathbf{F}^{\sigma\sigma'} = \nabla_{\mathbf{k}} \times \mathbf{A}^{\sigma\sigma'}$ for photons. In agreement with the helicity-degenerate light-cone spectrum of photons, the Berry curvature is diagonal, $\mathbf{F}^{\sigma\sigma'} = \delta^{\sigma\sigma'}\mathbf{F}^\sigma$, and it forms two monopoles at the Dirac-point origin of the momentum space (12–16):

$$\mathbf{F}^\sigma = \sigma\frac{\mathbf{k}}{k^3}, \quad \sigma = \pm 1 \qquad (2)$$

This curvature is responsible for the spin-redirection Berry phase and the SHE in optics (12–16).

We define the topological Chern numbers for the two helicity states $C^\sigma = \frac{1}{2\pi}\oint \mathbf{F}^\sigma d^2\mathbf{k}$, where the integral is taken over the $\mathbf{k}$-space sphere. The Chern numbers are meaningful in systems with Abelian Berry phases, such as 2D systems with the conserved spin component along the third dimension (7, 8, 28). This is also the case for photons having Abelian Berry phase, 2D polarization on the $\mathbf{k}$-space sphere, and conserved radial $\mathbf{k}$-component of the spin (helicity) (29). The monopole curvature (Eq. 2) yields $C^\sigma = 2\sigma$. The total

[1]Center for Emergent Matter Science, RIKEN, Wako-shi, Saitama 351-0198, Japan. [2]Nonlinear Physics Centre, Research School of Physics and Engineering, The Australian National University, Canberra, ACT 0200, Australia. [3]Department of Physics, University of Michigan, Ann Arbor, MI 48109-1040, USA.
*Corresponding author. E-mail: k.bliokh@gmail.com (K.Y.B.); fnori@riken.jp (F.N.)

Chern number $C = \sum\limits_{\sigma=\pm1} C^\sigma$ and the spin Chern number $C_{\text{spin}} = \sum\limits_{\sigma=\pm1} \sigma C^\sigma$ characterize the photonic QHE and QSHE properties [7, 8, 28]:

$$C = 0, C_{\text{spin}} = 4 \qquad (3)$$

The physical meaning of the Chern numbers is the number of edge modes with fixed direction of propagation. The vanishing total Chern number (Eq. 3) reflects the $\mathcal{T}$-symmetry of Maxwell equations and the absence of the QHE for free-space photons. At the same time, the nonzero spin Chern number (Eq. 3) implies that free-space light has two pairs of QSHE modes—edge counter propagating modes with opposite spins. Furthermore, the value $C_{\text{spin}} = 4$ implies that the topological $\mathbb{Z}_2$ invariant, associated with the $\mathcal{T}$-symmetry, vanishes: $\nu = \frac{C_{\text{spin}}}{2} \mod 2 = 0$. This means that surface modes of Maxwell equations are not helical fermions [30] as, for example, surface states of the Dirac equation [31, 32].

Nonetheless, nontrivial QSHE states of light exist, and they are well known. The photonic edge states of a bounded segment of free space are evanescent waves. For instance, assuming the $x = 0$ boundary, with free space at $x > 0$, the generic evanescent-wave solution of Maxwell equations can be written as [21]

$$\mathbf{E}_{\text{evan}} \propto \mathbf{e}_{\text{evan}} \exp(ik_z z - \kappa x),$$
$$\mathbf{e}_{\text{evan}} = \alpha\bar{\mathbf{x}} + \beta\frac{k}{k_z}\bar{\mathbf{y}} - i\alpha\frac{\kappa}{k_z}\bar{\mathbf{z}} \qquad (4)$$

Here, the spinor $\xi = (\alpha, \beta)^T$ still characterizes the wave polarization states. The wave (Eq. 4) propagates along the z axis with wave number $k_z > k$ and decays exponentially away from the boundary with decrement $\kappa = \sqrt{k_z^2 - k^2}$.

One can consider the evanescent wave (Eq. 4) as a plane wave with the complex wave vector $\mathbf{k} = k_z\bar{\mathbf{z}} + i\kappa\bar{\mathbf{x}}$. The transversality condition $\mathbf{E} \cdot \mathbf{k} = 0$ generates the imaginary longitudinal z-component in the polarization vector $\mathbf{e}_{\text{evan}}$, in contrast to the purely transverse polarization $\mathbf{e}$ in propagating waves (Eq. 1). This component produces a (x, z)–plane rotation of the electric or magnetic fields and generates unusual transverse spin in evanescent waves (Fig. 1) [20, 21]. This transverse spin is independent of the polarization ξ and can be written as

$$\mathbf{S}_\perp = \frac{\text{Re}\mathbf{k} \times \text{Im}\mathbf{k}}{(\text{Re}\mathbf{k})^2} \qquad (5)$$

Equation 5 demonstrates spin-momentum locking, similar to that in the QSHE and 3D topological insulators for electrons [5–8]. In particular, the z-propagating evanescent waves with $k_z > 0$ and $k_z < 0$ will have opposite transverse spins $S_y > 0$ and $S_y < 0$ (Figs. 2 to 4). Thus, any interface between free space and a medium supporting surface or guided modes with evanescent tails (Eq. 4) exhibits counter propagating opposite-spin edge modes—the QSHE of light. This is the first key point of our work.

In agreement with $C_{\text{spin}} = 4$, there are two pairs of QSHE modes in free space because the evanescent waves (Eq. 4) are double-degenerate with respect to the helicities $\sigma = \pm1$. However, the existence of surface modes in Maxwell equations requires a planar interface between the vacuum and a medium characterized by a permittivity ε and permeability μ. Such interface breaks the dual symmetry between the electric and magnetic properties: $\varepsilon \neq \mu$ [29]. This breaks the polarization degeneracy, and only a single polarization survives in the surface modes. For example, only transverse-magnetic surface waves exist at the interface with a medium with $\mu = 1$ and $\varepsilon < -1$. Calculating the spectrum, polarization, and spin of these surface modes of Maxwell equations, we obtain (supplementary text):

$$\omega_{\text{surf}} = \sqrt{\frac{1+\varepsilon}{\varepsilon}}\, k_{\text{surf}}, \xi_{\text{surf}} = \begin{pmatrix} 1 \\ 0 \end{pmatrix},$$
$$\langle\mathbf{S}_{\text{surf}}\rangle = \frac{1}{\sqrt{-\varepsilon}}\bar{\mathbf{k}}_{\text{surf}} \times \bar{\mathbf{n}}. \qquad (6)$$

Here, $\bar{\mathbf{k}}_{\text{surf}}$ and $\bar{\mathbf{n}}$ are the unit vectors of the propagation direction and the outer normal of the medium, respectively, and we calculated the mean (integral) spin per one surface-mode particle. The momentum-dependent spin $\langle\mathbf{S}_{\text{surf}}\rangle$ originates from the transverse spin (Eq. 5) of evanescent waves.

Equations. 5 and 6 determine the momentum locking of the spin $\mathbf{S}$ but not of the polarization spinor ξ (Fig. 2A). Polarization specifically corresponds to spin for nonrelativistic electrons, but for relativistic particles these are different notions. The surface modes of Maxwell equations have momentum-dependent spin $\mathbf{S}_{\text{surf}}$ but fixed spinor ξ_{surf} (Eq. 6). The latter corresponds to the trivial $\mathbb{Z}_2$ invariant $\nu = 0$ and shows that surface
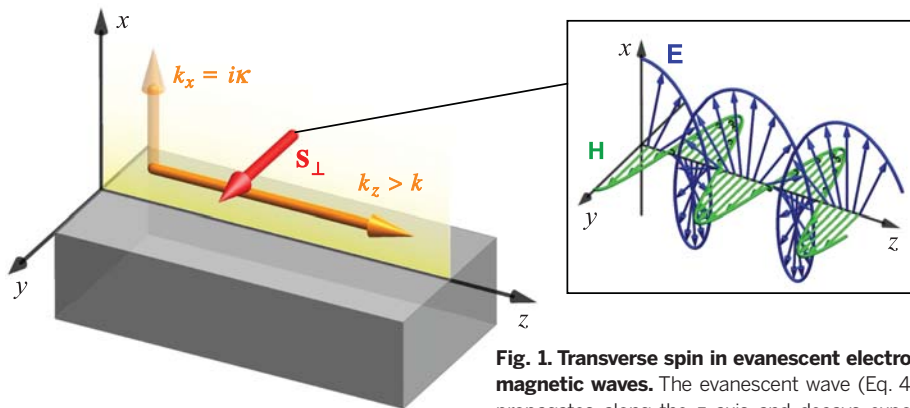

Fig. 1. Transverse spin in evanescent electromagnetic waves. The evanescent wave (Eq. 4) propagates along the z axis and decays exponentially in the $x > 0$ semi-space. (Inset) The instantaneous distributions of the electric and magnetic wave fields for the case of linear transverse-magnetic polarization, $\xi = (1, 0)^T$. The cycloidal (x, z)–plane rotation of the electric field generates the transverse spin $\mathbf{S}_\perp$ (Eq. 5) [20, 21]. The sign of the transverse spin depends on the direction of propagation of the evanescent wave.


Fig. 2. Spin and spinor properties of Maxwell and Dirac surface modes. (**A**) Surface modes of Maxwell equations propagating along the interface between the vacuum and a nontransparent medium with $\mu = 1$, $\varepsilon < -1$. These surface waves have fixed polarization $\xi_{\text{surf}} = (1, 0)^T$ but opposite transverse spins $\mathbf{S}$ locked to opposite wave momenta (Eqs. 5 and 6). (**B**) Topological surface modes of the Dirac equation at the interface between positive-mass and negative-mass regions [31, 32]. These modes exhibit locking between their momenta and spinors: Orthogonal polarizations propagate in opposite directions. However, the expectation value of their spin vanishes: $\mathbf{S}_{\text{surf}} = 0$ (supplementary text).
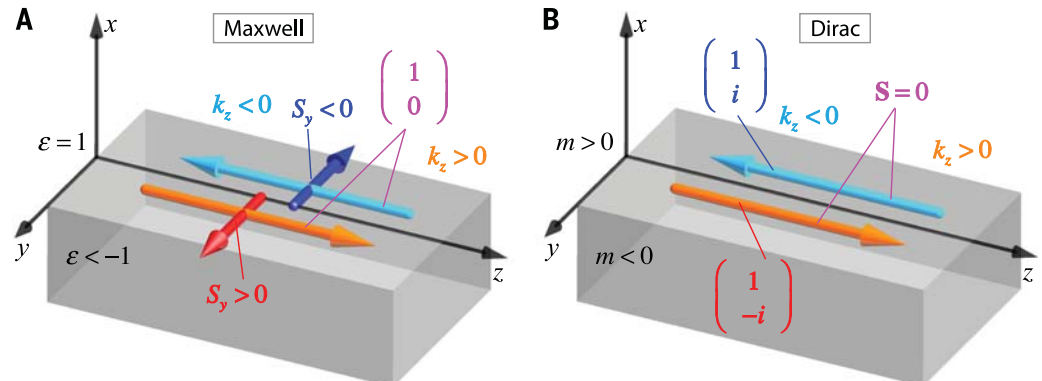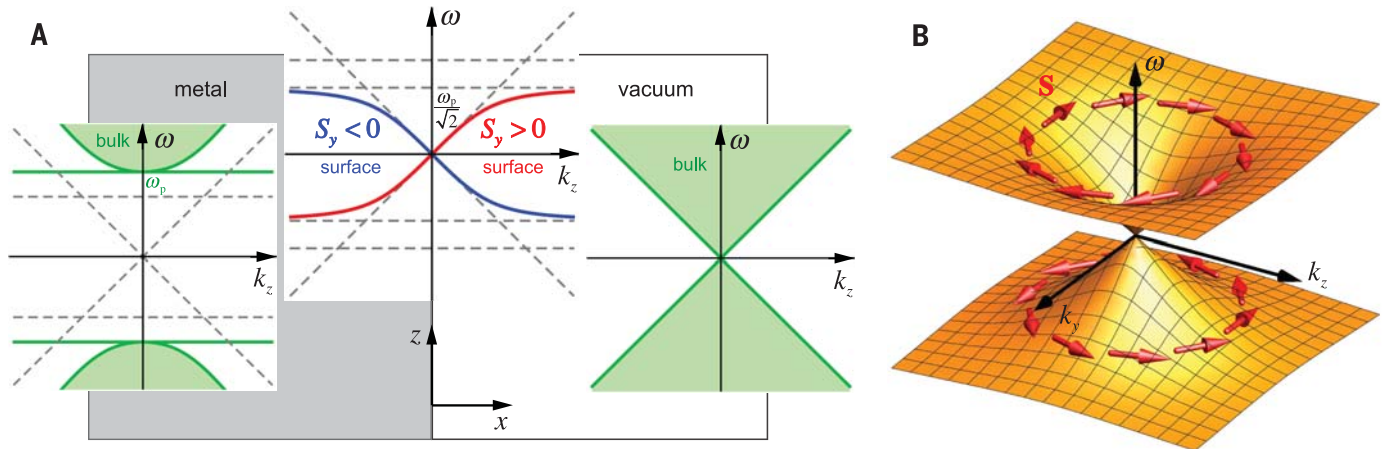
Fig. 3. Dispersion and spin-momentum locking of surface plasmon-polaritons. (**A**) Dispersion of bulk and surface modes at the vacuum-metal interface. SPPs exist inside the gap of the metal bulk spectrum and have spin-momentum locking associated with the transverse spin (Eqs. 5 and 6). (**B**) The two-dimensional dispersion of the same SPP mode exhibits a vortex spin texture similar to that for surface states of a 3D topological insulator (7, 8).
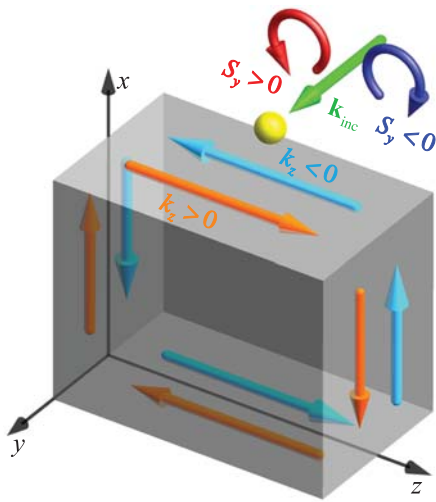
Fig. 4. Schematic of experiments demonstrating the QSHE of light. The incident y-propagating light (green) is coupled to surface modes with evanescent free-space tails via some scatterer (such as a nanoparticle). Depending on the spin of the incident light, $\mathbf{S}_{inc} = \sigma\overline{\mathbf{y}}$ (the helicity $\sigma = \pm 1$ is shown here by the circular-polarization arrows), surface waves with opposite propagation directions $\overline{\mathbf{k}}_{surf} = \pm\overline{\mathbf{z}}$ are excited (22–27).

Maxwell modes are bosons rather than helical fermions (30). Nonetheless, these modes provide the unidirectional edge spin transport (QSHE) because of the spin $\mathbf{S}_{surf}$. Precisely the opposite situation takes place in one of the main models for 3D electron topological insulators: the Dirac equation with surface modes at the interface between positive-mass and negative-mass regions (Fig. 2B) (31, 32). In this case, spinor-momentum locking occurs, which corresponds to the topological $\mathbb{Z}_2$ invariant $\nu = 1$. However, surprisingly, the expectation value of the spin of the surface Dirac modes vanishes because of the mutual cancellation of the polarization-dependent and

polarization-independent (similar to Eq. 5) contributions (supplementary text). Thus, one can say that surface Maxwell modes exhibit unidirectional spin transport (QSHE) but with trivial $\mathbb{Z}_2$ spinor properties, whereas the surface Dirac modes are topologically protected helical fermions that, however, do not transport spin. This is the second key point of our work.

Optical spin-momentum locking was recently observed in several experiments (22–27). An important example is provided by surface plasmon-polaritons (SPPs) at the vacuum-metal interface (33). Real metals are dispersive media with permittivity $\varepsilon(\omega) = 1 - \omega_p^2/\omega^2$, where ω_p is the plasma frequency. Metals are optical insulators at $\omega < \omega_p$, and at $\varepsilon < -1$ ($\omega < \omega_p/\sqrt{2}$), the vacuum-metal interface supports surface Maxwell modes—the SPPs (Fig. 3A). The metal becomes transparent at $\omega \geq \omega_p$, with bulk plasmons at $\omega = \omega_p$ and electromagnetic modes at $\omega > \omega_p$. As shown in Fig. 3A, the vacuum-metal interface resembles, by using condensed-matter analogies, the interface between a semimetal and an insulator. The SPP modes demonstrate spin-momentum locking (Eqs. 5 and 6) and nonremovable (because of the light-cone spectrum in vacuum) spectral degeneracy at $k = 0$, which are typical for electron QSHE states. Furthermore, plotting the SPP spectrum for a 2D surface of a 3D metal (Fig. 3B), one can see the conical spectrum and vortex spin texture analogous to those in 3D electron topological insulators (7, 8), but without the helical-fermion spinor properties (Fig. 2).

A schematic of the experiments (22–27) is shown in Fig. 4, revealing spin-controlled unidirectional transport in electromagnetic surface or guided waves. A transversely propagating free-space light beam with the usual spin $\mathbf{S}_{inc} = \sigma\overline{\mathbf{y}}$ (helicity $\sigma = \pm 1$) was coupled to the evanescent tails of the SPP or waveguide modes via some scatterer (such as a nanoparticle or an atom). In doing so, the opposite incident-spin states $\mathbf{S}_{inc} = \pm\overline{\mathbf{y}}$ excited the surface or guided modes running in the opposite directions: $\overline{\mathbf{k}}_{surf} = \pm\overline{\mathbf{z}}$. This spin-direction correlation reached almost

100% efficiency in various systems, independently of their details. This proves the universal spin-momentum locking in optical surface waves—the QSHE of light.

Thus, we have shown that light has intrinsic QSHE features, which arise from the spin-orbit interactions of photons. The corresponding spin-momentum locking originates solely from the basic properties of evanescent waves in Maxwell equations and can be observed at any interface with the vacuum, which supports surface or guided waves. In particular, surface plasmon-polaritons at a metal-vacuum interface exhibit features similar to those of surface states of topological insulators (vortex spin texture at the conical dispersion). Because of their trivial spinor structure, surface electromagnetic states are not helical fermions and are not protected from backscattering. Nonetheless, they do provide robust unidirectional spin transport. Our work shows that recent experiments, demonstrating highly efficient spin-controlled unidirectional excitation of surface or guided modes, can be interpreted as observations of the QSHE of light. The transverse spin locked to the direction of propagation seems to be a universal feature of surface vector waves of different nature. It appears in Maxwell and Dirac equations, as well as in Rayleigh surface waves in elastic media and surface-water waves. This offers robust angular-momentum-to-direction coupling in various surface waves as well as analogies and generalizations involving quantum and classical wave theories.

REFERENCES AND NOTES

1. M. Stone, Ed., *The Quantum Hall Effect* (World Scientific, Singapore, 1992).
2. D. J. Thouless, M. Kohmoto, M. P. Nightingale, M. den Nijs, *Phys. Rev. Lett.* **49**, 405–408 (1982).
3. S. Murakami, N. Nagaosa, S.-C. Zhang, *Science* **301**, 1348–1351 (2003).
4. J. Sinova et al., *Phys. Rev. Lett.* **92**, 126603 (2004).
5. C. L. Kane, E. J. Mele, *Phys. Rev. Lett.* **95**, 146802 (2005).
6. B. A. Bernevig, T. L. Hughes, S. C. Zhang, *Science* **314**, 1757–1761 (2006).
7. M. Z. Hasan, C. L. Kane, *Rev. Mod. Phys.* **82**, 3045–3067 (2010).
8. X.-L. Qi, S.-C. Zhang, *Rev. Mod. Phys.* **83**, 1057–1110 (2011).

9. G. L. J. A. Rikken, B. A. van Tiggelen, *Nature* **381**, 54–55 (1996).
10. F. D. M. Haldane, S. Raghu, *Phys. Rev. Lett.* **100**, 013904 (2008).
11. Z. Wang, Y. Chong, J. D. Joannopoulos, M. Soljačić, *Nature* **461**, 772–775 (2009).
12. R. Y. Chiao, Y.-S. Wu, *Phys. Rev. Lett.* **57**, 933–936 (1986).
13. K. Y. Bliokh, Y. P. Bliokh, *Phys. Lett. A* **333**, 181–186 (2004).
14. M. Onoda, S. Murakami, N. Nagaosa, *Phys. Rev. Lett.* **93**, 083901 (2004).
15. K. Y. Bliokh, A. Niv, V. Kleiner, E. Hasman, *Nat. Photonics* **2**, 748–753 (2008).
16. K. Y. Bliokh, M. A. Alonso, E. A. Ostrovskaya, A. Aiello, *Phys. Rev. A* **82**, 063825 (2010).
17. M. Hafezi, E. A. Demler, M. D. Lukin, J. M. Taylor, *Nat. Phys.* **7**, 907–912 (2011).
18. A. B. Khanikaev *et al.*, *Nat. Mater.* **12**, 233–239 (2013).
19. M. C. Rechtsman *et al.*, *Nature* **496**, 196–200 (2013).
20. K. Y. Bliokh, F. Nori, *Phys. Rev. A* **85**, 061801 (2012).
21. K. Y. Bliokh, A. Y. Bekshaev, F. Nori, *Nat. Commun.* **5**, 3300 (2014).
22. F. J. Rodríguez-Fortuño *et al.*, *Science* **340**, 328–330 (2013).
23. J. Petersen, J. Volz, A. Rauschenbeutel, *Science* **346**, 67–71 (2014).
24. D. O'Connor, P. Ginzburg, F. J. Rodríguez-Fortuño, G. A. Wurtz, A. V. Zayats, *Nat. Commun.* **5**, 5327 (2014).
25. R. Mitsch, C. Sayrin, B. Albrecht, P. Schneeweiss, A. Rauschenbeutel, *Nat. Commun.* **5**, 5713 (2014).
26. B. le Feber, N. Rotenberg, L. Kuipers, *Nat. Commun.* **6**, 6695 (2015).
27. I. Söllner *et al.*, arXiv:1406.4295v3 (2014).
28. D. N. Sheng, Z. Y. Weng, L. Sheng, F. D. M. Haldane, *Phys. Rev. Lett.* **97**, 036808 (2006).
29. I. Fernandez-Corbaton *et al.*, *Phys. Rev. Lett.* **111**, 060401 (2013).
30. L. Lu, J. D. Joannopoulos, M. Soljačić, *Nat. Photonics* **8**, 821–829 (2014).
31. R. Jackiw, C. Rebbi, *Phys. Rev. D Part. Fields* **13**, 3398–3409 (1976).
32. A. P. Schnyder, S. Ryu, A. Furusaki, A. W. W. Ludwig, *Phys. Rev. B* **78**, 195125 (2008).
33. A. V. Zayats, I. I. Smolyaninov, A. A. Maradudin, *Phys. Rep.* **408**, 131–314 (2005).

3D LITHOGRAPHY

Atomic gold–enabled three-dimensional lithography for silicon mesostructures

Zhiqiang Luo,[1]* Yuanwen Jiang,[1]* Benjamin D. Myers,[2,3] Dieter Isheim,[2,4] Jinsong Wu,[2,3] John F. Zimmerman,[1] Zongan Wang,[1] Qianqian Li,[2,3] Yucai Wang,[5] Xinqi Chen,[2,3] Vinayak P. Dravid,[2,3] David N. Seidman,[2,4] Bozhi Tian[1,5,6]†

Three-dimensional (3D) mesostructured semiconductors show promising properties and applications; however, to date, few methods exist to synthesize or fabricate such materials. Metal can diffuse along semiconductor surfaces, and even trace amounts can change the surface behavior. We exploited the phenomena for 3D mesoscale lithography, by showing one example where iterated deposition-diffusion-incorporation of gold over silicon nanowires forms etchant-resistant patterns. This process is facet-selective, producing mesostructured silicon spicules with skeletonlike morphology, 3D tectonic motifs, and reduced symmetries. Atom-probe tomography, coupled with other quantitative measurements, indicates the existence and the role of individual gold atoms in forming 3D lithographic resists. Compared to other more uniform silicon structures, the anisotropic spicule requires greater force for detachment from collagen hydrogels, suggesting enhanced interfacial interactions at the mesoscale.

Semiconductors with three-dimensional (3D) mesoscale features (*1–5*) are an emerging class of materials, with promising applications from stretchable bioelectronics (*3*) to alternative plasmonics and metamaterials (*6*). However, progress in this area has been impeded by challenges in chemical synthesis (*5*) and limitations in 3D fabrication methods

(*1, 2, 4, 7*). As a result, this area would benefit from new synthetic concepts or new components in lithography. One place to look for such inspiration is in biomaterials-based processes, which routinely assemble mesostructured materials.

In the growth of natural hard biomaterials, trace amounts of interfacial organic species are important components (*8*), yielding unusual 3D biomaterial shapes and properties. The application of trace organic molecules as components (e.g., an etching resist) in semiconductor-based lithography is hard to achieve, given that semiconductor processing typically involves either high-temperature gas-phase or harsh solution-phase preparations. However, inorganic species are much more stable and can be introduced as trace components into various semiconductors, as either impurities in the bulk volume (*9–11*) or as diffused species near the surface (*12–16*), with the latter holding great potential in 3D semi-

conductor lithography, given that surface diffusion is versatile and more controllable.

Here we focus on 3D mesoscale lithography of silicon (Si) nanowires with diffused gold (Au) (*13, 14, 17*), where Au originates from the nanoparticle catalyst used for nanowire nucleation and elongation [Fig. 1, supplementary materials (*18*), and fig. S1]. Because Au diffusion over Si surfaces is pressure-dependent (*16*), we first adopted periodic pressure modulation during Au-catalyzed Si nanowire synthesis to develop Au diffusion–induced patterns along nanowire sidewalls (figs. S1 to S3), where silane (SiH_4) and diborane (B_2H_6) were used as a Si precursor and a *p*-type dopant, respectively. Next, we revealed the Au-based patterns with anisotropic wet chemical etching in KOH solutions [materials and methods (*18*) and fig. S4]. The as-grown Si structures have rather uniform diameters except for periodic swells at the evacuation locations (figs. S2 and S3). After etching, we identified two Si mesostructures from the same growth batch: a type I spicule with platelike nodes and a type II spicule with triangle-shaped nodes (Fig. 1, A and B). Portions of the nanowire surfaces remained after etching, suggesting that the diffused Au acted as an etching resist. Both spicule structures show gradient, curved, and anisotropic surface textures. These formations are reminiscent of other complex nanowire morphologies (*19–24*) but are also similar to some naturally occurring hard materials, such as skeletons (*8*).

Transmission electron microscopy (TEM) images of *p*-type Si spicules (Fig. 1, C to F, and fig. S5) show that type I and type II structures grow along the <111> and <112> directions, respectively. Although type I is a single crystal, the type II spicule has a {111} twin plane (*11*), which separates subunits α and β (Fig. 1F, TB marks the twin boundary), as determined by the two sets of diffraction spots (Fig. 1F, magenta/white and blue/white dashed circles) in the selected area electron diffraction (SAED) pattern.

We used scanning TEM (STEM) for tomograms of mesostructured Si spicules (*18*) (Fig. 2, A and B, and fig. S6). In addition to the expected structural gradient and anisotropy, we revealed convex and

[1]Department of Chemistry, the University of Chicago, Chicago, IL 60637, USA. [2]Department of Materials Science and Engineering, Northwestern University, Evanston, IL 60208, USA. [3]Northwestern University Atomic and Nanoscale Characterization Experimental (NUANCE) Center, Northwestern University, Evanston, IL 60208, USA. [4]The Northwestern University Center for Atom-Probe Tomography (NUCAPT), Northwestern University, Evanston, IL 60208, USA. [5]The James Franck Institute, the University of Chicago, Chicago, IL 60637, USA. [6]The Institute for Biophysical Dynamics, Chicago, IL 60637, USA.
*These authors contributed equally to this work. †Corresponding author. E-mail: btian@uchicago.edu

Quantum spin Hall effect of light
Konstantin Y. Bliokh *et al.*
Science **348**, 1448 (2015);
DOI: 10.1126/science.aaa9519